

Novel Ferrocenyl-Substituted Organometallics with Pyrimidine Moiety as Potent Antiprotozoal Agents: Synthesis, Characterization and *in silico* Evaluation

HUMAIRA PARVEEN^{1,*}, MOHAMMAD YOUNUS WANI², FATIMAH A. ALOTAIBI¹, SAYEED MUKHTAR¹ and UZMA FARIDI³

¹Department of Chemistry, Faculty of Science, University of Tabuk, Tabuk-71491, Kingdom of Saudi Arabia

²Department of Chemistry, College of Science, University of Jeddah, 21589 Jeddah, Kingdom of Saudi Arabia

³Department of Biochemistry, Faculty of Science, University of Tabuk, Tabuk-71491, Kingdom of Saudi Arabia

*Corresponding author: Tel: +966 144567227; E-mail: h.nabi@ut.edu.sa

Received: 3 June 2023;

Accepted: 19 July 2023;

Published online: 31 August 2023;

AJC-21363

Metallo drugs have been extensively used in modern research to design and synthesize new core drug molecules. In search of new leads in protozoal chemotherapy, novel ferrocene-substituted pyrimidine-based organometallic compounds has been synthesized and thoroughly investigated their ADMET (absorption, distribution, metabolism, excretion and toxicity) and pharmacokinetic properties. The compounds exhibited excellent solubility potential, with favourable permeability and absorption characteristics. They demonstrated low toxicity, as indicated by clearance values and oral toxicity measurements. Molecular docking studies revealed strong interactions with the target site, surpassing the performance of reference drugs metronidazole and ornidazole. Overall, these organometallic compounds possess desirable ADMET profiles, meet Lipinski's criteria and exhibit promising drug-likeness properties, positioning them as potential leads for the development of effective antiprotozoal agents.

Keywords: Ferrocene, Substituted organometallics, Pharmacokinetic, Molecular docking studies, Antiprotozoal, Chemotherapy.

INTRODUCTION

Amoebiasis (amoebic dysentery) is a deadly human gastrointestinal tract disease, caused by *Entamoeba histolytica* (a protozoan parasite). Every year around 100,000 fatalities have been reported worldwide due to this infectious disease [1]. However, successful treatment of amoebiasis is available by nitroimidazoles such as metronidazole, tinidazole and ornidazole [2-4] but these drugs are reported to have adverse side effects [5]. Moreover, metronidazole has been reported carcinogenic in rodents and also found to cause spermatozoid destruction, gastric mucus lining irritation, convulsions, disorders of the central nervous system and hematuria [6-10]. Also, frequent emergence of drug resistance towards conventional medicines for amoebiasis has been reported [11]. Therefore, it is necessary to work in search of potent, safer and efficacious drugs for the protozoal chemotherapy.

Potential applications of ferrocenyl-substituted organometallics in pharmacology have been extensively explored in recent years. Also, metal-embedded heterocyclic compounds/

bio-organometallics offer the potential to develop new antiprotozoal agents and possess an impressive track record in antiprotozoal and in anticancer drug development, such as ferrocifen [12,13], hydroxyferrocifen [14,15], JAHA, cisplatin [16], ruthenocifen [17] and ferroquine [18] are testimony to these developments.

Ferrocene-embedded organometallic compounds have been reported to possess multi-therapeutic potential due to the unique properties and activities of ferrocene which act as an excellent pharmacophore for drug discovery [19]. Ferroquine (chloroquine derivative, containing a ferrocenyl group) is the best example of the role of ferrocene in drug discovery. Ferroquine is proven to be a drug to treat malaria and currently undergoing phase III clinical studies. Ferrociphenol [20] and ferrocene-embedded estradiol [21] have been reported excellent antiproliferative activities. Moreover, nitrogen-containing heterocycles such as pyrimidines are major heterocyclic rings in the structures of nucleic acids thereby essential for many biological functions. Pyrimidines are also an integral part of many antiviral drugs, for example, zidovudine and lamivudine

are used to treat HIV infection and also constitute attractive scaffolds for drug discovery by exhibiting excellent biological activities such as antimalarial [22], anticancer [23,24], anti-tumor [25], antitubercular [26], antiviral [27] and as potent epidermal growth factor receptor (EGFR) inhibitors [28].

In view of the above extensive literature survey regarding the metal-embedded heterocyclic compounds and our dedicated work towards the discovery of novel organometallic compounds and heterocyclic compounds [29-35], we have designed and synthesized novel ferrocene-embedded organometallic compounds with pyrimidine moiety with an objective to evaluate their ADMET, pharmacokinetic and docking studies to develop more potent antiprotozoal agents.

EXPERIMENTAL

All chemicals including substituted aromatic aldehydes, 2-acetylferrocene and reagents were acquired from Sigma-Aldrich. TLC technique was performed on commercially available TLC sheets obtained from Merck, Germany. Subsequently, the visualization of the separated compounds on the TLC plates was achieved using a UV lamp. Stuart SMP10 capillary melting apparatus was used to record melting points. Thermo-Scientific Nicolet [model iS5 FT-IR spectrophotometer] was used to record IR spectra by using KBr discs. Bruker AVANCE 400 spectrometer was used to record ^1H NMR and ^{13}C NMR spectra and the compounds were dissolved in DMSO. Trimethylsilane (TMS) an internal standard was used for NMR analysis and chemical shifts (δ) were observed in ppm.

Synthesis of ferrocene-embedded chalcones (1a-d): The starting materials [ferrocene-embedded chalcones (1a-d)] were synthesized as per reported method [29]. In a round bottom flask, 6 mmol of aromatic ketone mixed with 0.4 g of KOH was dissolved in 10 mL of absolute ethanol and then stirred for 15 min at room temperature (25 °C). After that, ferrocene carboxaldehyde (6 mmol) dissolved in 10 mL of absolute ethanol was added dropwise to the reaction mixture. The reaction mixture was further stirred at 25 °C. A precoated TLC plate was used to monitor the progress of the reaction. As per TLC indication, about the formation of chalcones, 2 M HCl was used to neutralize the reaction mixture, which precipitated the chalcones. The ferrocene-embedded chalcones were filtered and washed several times with water and dried under vacuum to yield pure respective ferrocene-embedded chalcone.

Synthesis of 4-methylpiperidine-1-carboxamide hydrochloride (2): Imidine hydrochloride [4-methyl piperidine-1-carboxamide hydrochloride (2)] was synthesized as per reported procedure [36]. To synthesize (2) 4-methyl piperidine was refluxed with aqueous 2-methyl-2-thiopseudourea hemisulfate salt.

Synthesis of ferrocene-embedded organometallics with pyrimidine moiety (3a-d): A solution of 2.0 equiv. of 4-methylpiperidine-1-carboxamide hydrochloride (2) was prepared in 50 mL isopropanol, then 2.2 equiv. of sodium metal was incorporated into this solution and subjected to reflux for 2 h after that addition of 2.0 equiv. of ferrocenyl substituted chalcone (1a-d) was done and the reaction mixture was further refluxed. The reaction's progress was checked by precoated TLC. As

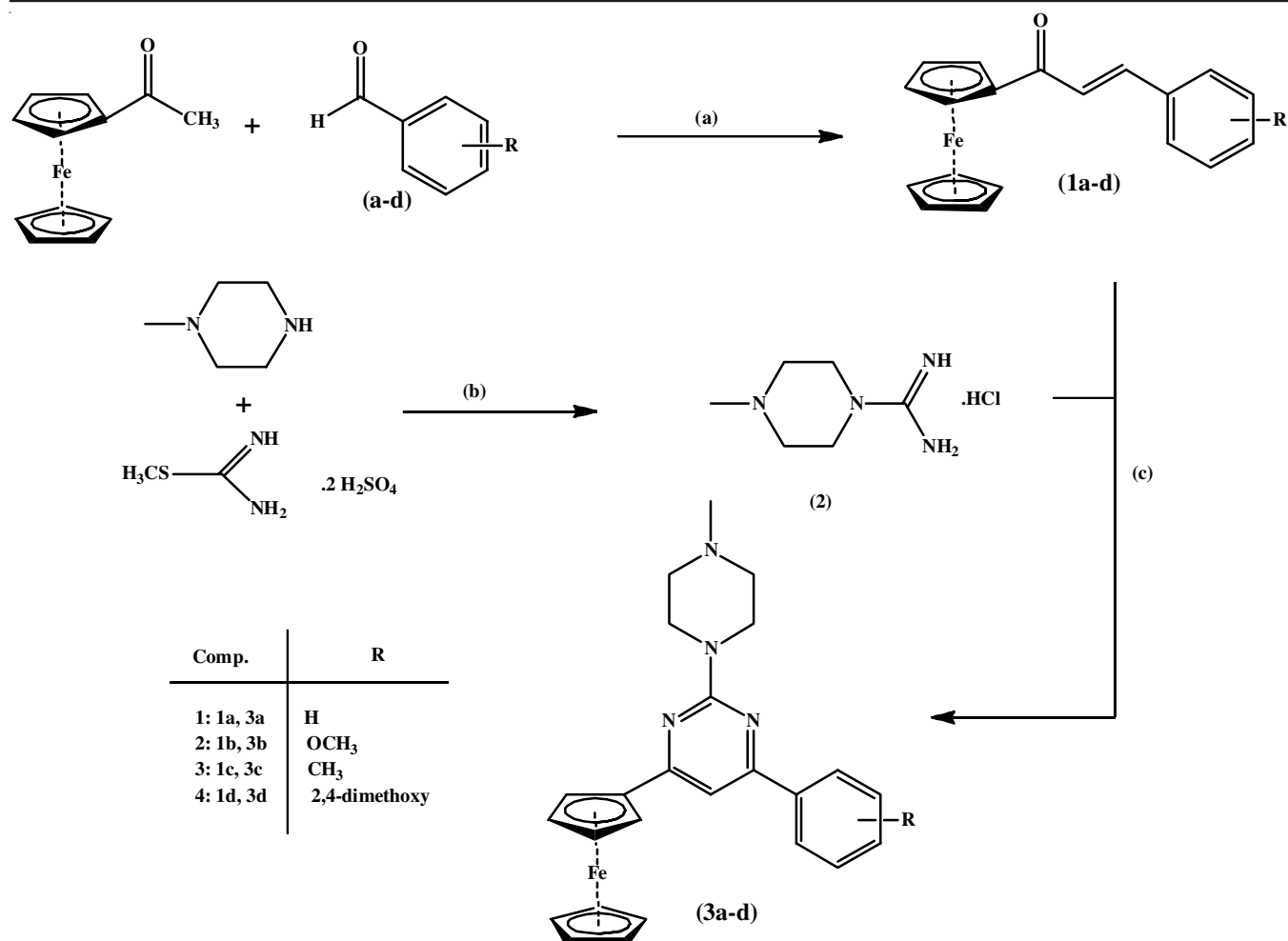
per TLC indication about the product formation, the solvent was removed under vacuum. Then after the addition of water to the reaction mixture, it was extracted with CHCl_3 and then 10% NaCl solution was added to it. The chloroform layer was dried by using anhydrous Na_2SO_4 and the solvent was evaporated in a rotatory evaporator. The crude products were crystallized by using ethanol which afforded, corresponding pure ferrocene-embedded organometallics with pyrimidine moiety (Scheme-I).

4-Phenyl-2-(4-methylpiperidin-1-yl)-6-ferrocenyl pyrimidine (3a): Dark maroon; Yield: 72%; m.p.: 129 °C; Elemental analysis calcd. (found) % of $\text{C}_{26}\text{H}_{27}\text{N}_3\text{Fe}$: C, 71.40 (69.89); H, 6.22 (6.24); N, 9.61 (9.59). IR (KBr, ν_{max} , cm^{-1}): 3096, 2922, 1651, 1492, 1276; ^1H NMR (DMSO) δ ppm: 7.36 (s, 1H, Py-ring), 7.01-7.35 (m, 5H, ph-ring), 74.84 (s, 2H, cp), 4.55 (s, 2H, cp), 4.21 (m, 5H, cp), 4.00 (t, 4H, $2\times\text{CH}_2$, piperidine), 2.96 (t, 4H, $2\times\text{CH}_2$, piperidine), 2.38 (s, 3H, piperidine); ^{13}C NMR (DMSO) δ ppm: 164.3 (C=N), 162.5 (C=C), 162.0 (N=C-N), 141.5-120.3 (aromatic C), 111.5 (C-H pyrimidine), 79.7 (*ipso*- C_5H_4), 72.6, 70.1 (*meta*- C_5H_4), 68.6, 69.5 (C_5H_5), 68.6, 69.5 (*ortho*- C_5H_4), 66.4 (C-C-C piperidine ring), 41.6 (C-N-C piperidine ring), 27.6 ($-\text{CH}_3$ piperidine ring). ESI-MS m/z : [$\text{M}^+ + 1$] 438.36.

4-(2,4-Dimethoxy phenyl)-6-ferrocenyl-2-(4-methylpiperidin-1-yl)-pyrimidine (3b): Brick-red coloured, yield: 77%; m.p.: 144 °C. Elemental analysis calcd. (found) % of $\text{C}_{28}\text{H}_{31}\text{N}_3\text{O}_2\text{Fe}$: C, 67.61 (68.62); H, 6.28 (6.25); N, 8.45 (8.48); O, 6.43 (6.40). IR (KBr, ν_{max} , cm^{-1}): 3096, 2921, 1496, 1455, 1279, 114.8; ^1H NMR (DMSO) δ ppm: 7.69-8.20 (m, 5H, ph-ring), 7.38 (s, 1H, Py-ring), 4.97 (s, 2H, cp), 4.68 (s, 2H, cp), 4.22 (m, 5H, cp), 4.02 (t, 4H, $2\times\text{CH}_2$, piperidine), 2.51 (t, 4H, $2\times\text{CH}_2$, piperidine), 2.37 (t, 3H, piperidine); ^{13}C NMR (DMSO) δ ppm: 164.0 (C=N), 162.4 (C=C), 162.1 (N=C-N), 141.3-122.0 (aromatic C), 104.5 (C-H pyrimidine), 79.7-79.6 (*ipso*- C_5H_4), 72.6, 70.1 (*meta*- C_5H_4), 68.6, 69.5 (C_5H_5), 70.01, 69.9 (*ortho*- C_5H_4), 66.6 (C-C-C piperidine ring), 56.6, 55.4 ($2\times\text{OCH}_3$ phenyl ring), 43.9 (C-N-C piperidine ring), 27.7 ($-\text{CH}_3$ piperidine ring). ESI-MS m/z : [$\text{M}^+ + 1$] 497.41.

4-(4-Chloro phenyl)-6-ferrocenyl-2-(4-methylpiperidin-1-yl)-pyrimidine (3c): Maroon coloured, yield: 68%; m.p.: 377 °C. Elemental analysis calcd. (found) % of $\text{C}_{26}\text{H}_{26}\text{ClN}_3\text{Fe}$: C, 66.19 (66.22); H, 5.55 (5.51); Cl, 7.51 (7.58); N, 8.91 (8.93). IR (KBr, ν_{max} , cm^{-1}): 3096, 2921, 1577, 1489, 1276; ^1H NMR (DMSO) δ ppm: 7.55-8.19 (m, 5H, ph-ring), 7.35 (s, 1H, Py-ring), 4.89 (s, 2H, cp), 4.66 (s, 2H, cp), 4.22 (m, 5H, cp), 4.01 (t, 4H, $2\times\text{CH}_2$, piperidine), 2.55 (t, 4H, $2\times\text{CH}_2$, piperidine), 2.33 (s, 3H, piperidine); ^{13}C NMR (DMSO) δ ppm: 164.2 (C=N), 162.2 (C=C), 161.5 (N=C-N), 141.1-122.0 (aromatic C), 111.2 (C-H pyrimidine), 79.7 (*ipso*- C_5H_4), 72.5, 70.1 (*meta*- C_5H_4), 68.6, 69.8 (C_5H_5), 68.6, 69.5 (*ortho*- C_5H_4), 66.2 (C-C-C piperidine ring), 40.9 (C-N-C piperidine ring), 27.5 ($-\text{CH}_3$ piperidine ring). ESI-MS m/z : [$\text{M}^+ + 1$] 472.80.

4-(4-Methoxy phenyl)-6-ferrocenyl-2-(4-methylpiperidin-1-yl)-pyrimidine (3d): Brick-red, yield: 78%; m.p.: 216 °C. Elemental analysis calcd. (found) % of $\text{C}_{27}\text{H}_{29}\text{N}_3\text{OFe}$: C, 69.38 (69.35); H, 6.25 (6.22); N, 8.99 (8.97); O, 3.42 (3.40). IR (KBr, ν_{max} , cm^{-1}): 3096, 2917, 1510, 1455, 1279, 114.2; ^1H NMR (DMSO) δ ppm: 7.65-8.21 (m, 5H, ph-ring), 7.33 (s,



Scheme-I: Synthesis of ferrocene-embedded organometallic compounds with pyrimidine moiety. Reagents and conditions: (a) 10% aq. NaOH, absolute EtOH, rt, 30 min, (b) i. 4-methyl piperidine, S-methylisothiourea sulfate, water, reflux, 15 min. ii. BaCl₂, reflux, 15 min, (c) 4-methylpiperidine-1-carboxamide hydrochloride, sodium isopropoxide, isopropanol, reflux, 6-8 h

1H, Py-ring), 4.88 (s, 2H, cp), 4.64 (s, 2H, cp), 4.12 (m, 5H, cp), 4.05 (t, 4H, 2×CH₂, piperidine), 3.87 (s, 3H, -OCH₃), 2.55 (t, 4H, 2×CH₂, piperidine), 2.38 (t, 3H, piperidine); ¹³C NMR (DMSO) δ ppm: 164.2 (C=N), 162.1 (C=C), 160.1 (N=C-N), 140.0-122.2 (Ar-C), 111.2 (C-H Py-ring), 79.7-79.5 (ipso-C₅H₄), 72.6, 70.2 (*meta*-C₅H₄), 68.3, 69.8 (C₅H₅), 70.01, 69.9 (*ortho* C₅H₄), 66.2 (C-C-C piperidine ring), 55.1 (-OCH₃ phenyl ring), 41.0, (C-N-C piperidine ring), 27.6 (-CH₃ piperidine ring). ESI-MS *m/z*: [M⁺ + 1] 468.38.

Molecular docking studies: The crystal structure of thioredoxin reductase from *Entamoeba histolytica* (PDB ID: 4CCQ) at a resolution of 1.50 Å was obtained from the protein data bank. Molecular operating environment (MOE) software was employed for docking analysis. To prepare the target proteins, water molecules were removed, leaving only one chain necessary for binding. The reference ligand was co-crystallized and hydrogen atoms were hidden while protonating the protein structures. The energy minimization of the protein structures was performed using the MMFF94x force field and the binding pocket of the target protein was defined using predefined MOE settings. The structures of the organometallic compounds (**3a-d**) were drawn using ChemBioDraw Ultra 14.0 and saved in SDF

format. The files were then imported into MOE and the 3D structures were protonated and energy-minimized using the MMFF94x force field. The validation of the target receptor was conducted by docking the co-crystallized ligand and assessing the RMSD values between the docked and crystal conformations. The results from MOE software were further analyzed and visualized using both MOE and Discovery Studio 4.0 software tools.

RESULTS AND DISCUSSION

Chemistry of ferrocene-embedded organometallics: The synthesis of the aforementioned novel ferrocene-embedded organometallics (**3a-d**) has been furnished in three steps and depicted in **Scheme-I**. The first step includes the synthesis of ferrocenyl substituted α,β -unsaturated ketones (**1a-d**), which were prepared by the reported method [29], in brief, by the alcoholic KOH-induced reaction of 2-acetyl ferrocene with various substituted aromatic aldehydes. The second step includes the synthesis of 4-methylpiperidine-1-carboxamide hydrochloride (**2**), which was synthesized by refluxing 4-methyl piperidine with aqueous 2-methyl-2-thiopseudourea hemi-sulfate salt [37]. The corresponding ferrocene-embedded organo-

metallic compounds (**3a-d**) were obtained by the cyclization of ferrocenyl substituted α,β -unsaturated ketones (**1a-d**) with 4-methylpiperidine-1-carboxamide hydrochloride (**2**) by using sodium metal and isopropanol. The structures of all the novel ferrocene-embedded organometallics have been established by performing spectral studies and elemental analyses of respective organometallics.

The formation of ferrocene-embedded organometallics (**3a-d**) is significantly indicated by characteristic IR bands. The absorption band for C=N stretch was observed in all the novel organometallics within the range of 1577-1496 cm^{-1} , confirming the cyclization of ferrocenyl-substituted ketones with 4-methylpiperidine-1-carboxamide hydrochloride affording corresponding organometallics with pyrimidine ring. Additionally, the absorption bands for the -CN group were observed in the region of 1279-1276 cm^{-1} further confirming the formation of the targeted pyrimidine unit in all ferrocene-embedded organometallic compounds. Proton NMR and Carbon-13 NMR studies of the target compounds (**3a-d**) were further corroborating their structures. The characteristic single proton (C-H proton of pyrimidine moiety) has appeared within the range of δ 7.33-7.42 ppm as a singlet in all the synthesized ferrocene-embedded organometallics. Additionally, the protons (4 H) of monosubstituted Cp of ferrocene unit exhibited three singlets ranging from δ 4.88-5.50, 4.64-4.68 and 4.60-4.62 ppm and the five protons of unsubstituted Cp showed characteristic singlet ranging from δ 4.12-4.22 ppm in all the synthesized organometallics. The protons of all aromatic rings, ferrocenyl group and 4-methylpiperidine ring have shown chemical shift values at their expected region.

The ^{13}C NMR spectra of the aforementioned target compounds (**3a-d**) were more informative about the assigned structures. It showed a sharp signal ranging from δ 164.0-164.2 ppm ascribable to the C=N group and a characteristic signal in the range of δ 162.1-162.5 ppm was attributed to C=C, which provided further proof for the formation of ferrocene-embedded organometallics. The characteristic signal for the carbon of the pyrimidine ring bearing hydrogen appeared in the range of δ 104.5-111.2 ppm, in all organometallics providing the confirmation of closure of the ring to form pyrimidine moiety. The values of other signals attributed to the carbons of the aromatic

ring, ferrocenyl group and 4-methylpiperidine ring moieties, resonated at their usual regions.

Pharmacokinetic/ADMET (absorption, distribution, metabolism, excretion and toxicity) studies: To assess the drug-like potential of the newly synthesized molecules, ADMET and pharmacokinetic properties have been investigated. The prediction tools used for this analysis included pkCSM, an online resource provided by the University of Cambridge and MedChemDesignerTM software version 3.0 [38], which is known for its precise value predictions. The predicted values for the organometallics **3a-d** indicated favourable drug-like properties. The solubility potential of the molecules was found to be within a desirable range, both in water (log mol/L) (-3.90 to 3.23) and CaCO_2 permeability (log Papp in 10 cm/s) (1.22 to 1.01) (Table-1).

The solubility at pH 7.4 and intrinsic water solubility was observed at -3.25 to -3.45. The molecules exhibited approximately 85% intestinal absorption in humans and their skin permeability was estimated to be around -2.73 (log Kp). In terms of brain assay (BBB permeability) and CNS permeability were found -0.10 to 0.46 (log BB) and -2.24 to -2.03, respectively. The clearance values, which represent the drug elimination rate relative to the concentration of its plasma, were observed quite favourable for all organometallics (-0.16 to -2.04 log mL/min/kg). This suggests that in the body these organometallics would not accumulate, thereby, indicating their non-toxic and non-hepatotoxic properties. Furthermore, The range of oral rat acute toxicity (LD_{50}) was observed 3.17 to 2.62 mol/kg and the range of oral rat chronic toxicity (LOAEL) was found 1.55 to 0.30 (log mg/kg bw/day) with the range of 0.59 to 0.10 log mg/kg/day being a maximum tolerated dose in human drug-like characteristics. The results of all these studies revealed that these organometallics demonstrated excellent ADMET characteristics, which are crucial for exhibiting drug-like characteristics.

In the assessment of drug-like properties, the predicted pharmacokinetic parameters and adherence to Lipinski's filters play a crucial role, both in computational (*in silico*) and experimental (*in vitro*) evaluations [39-41]. These parameters serve as important criteria in the later stages of drug development. A molecule that does not meet the required pharmacokinetic parameters and fails to comply with Lipinski's filters may face challenges in advancing further. Upon evaluating the predicted

TABLE-1
ADMET PARAMETERS OF THE SYNTHESIZED ORGANOMETALLIC COMPOUNDS (**3a-d**) AND REFERENCE DRUGS

ADMET parameters	3a	3b	3c	3d	Metronidazole	Ornidazole (Positive controls)
Water solubility	-3.90	-3.30	-3.23	-3.33	-2.12	-2.03
CaCO_2 permeability	1.04	1.22	1.06	1.01	0.51	0.68
Intestinal absorption	87.36	89.44	84.75	89.50	92.75	92.76
Skin permeability	-2.73	-2.73	-2.73	-2.72	-2.79	-2.76
BBB permeability	0.37	0.46	0.27	-0.10	-0.73	-0.94
CNS permeability	-2.03	-2.24	-1.97	-2.23	-3.00	-3.45
Total clearance	-1.95	-2.13	-0.16	-2.04	0.48	0.84
Oral rat acute toxicity (LD_{50})	2.91	3.36	2.62	3.17	1.75	2.05
Oral rat chronic toxicity (LOAEL)	1.55	0.66	0.30	0.71	1.44	1.33
Max. tolerated dose (human)	0.18	0.59	0.10	0.16	-0.29	-0.37
Hepatotoxicity	No	No	No	No	No	No
AMES toxicity	No	No	No	No	No	No

pharmacokinetic parameters and by employing Lipinski's filters, it is evident that all the organometallics exhibit favourable drug-like properties (Table-2). This indicates that these compounds have the potential to be promising drug-like candidates for further studies and development in antiprotozoal chemotherapy.

From the bioavailability radar of the organometallic compounds, obtained from SwissADME, it was observed that certain molecules displayed excellent physico-chemical characteristics for oral bioavailability. The assessment was based on six essential physicochemical parameters, namely polarity, size, solubility, lipophilicity, flexibility and saturation. For instance, the oral bioavailability of compounds **3a-d** was evaluated and their physico-chemical profiles were found to fall within the pink-coloured region as depicted in Fig. 1 [42,43]. The pink area represents the optimal range for each property, including lipophilicity (XLOGP3: -0.7 to +5.0), size (MW: 150 to 500 g/mol), polarity (TPSA: 20 to 130 Å²), solubility

(log S ≤ 6), saturation (fraction of carbons in *sp*³ hybridization ≥ 0.25) and flexibility (up to 9 rotatable bonds). A molecule is considered to have drug-like characteristics if its radar plot lies entirely within the pink area.

During various stages of the drug discovery process, it is crucial to assess gastrointestinal absorption and brain access as important pharmacokinetic parameters. Introducing the Brain or IntestinaL EstimateD permeation method (BOILED-Egg) as an accurate predictive model, it calculates the lipophilicity and polarity of small molecules, providing valuable support for lead optimization. The BOILED-Egg model concurrently predicts two key ADME parameters: passive gastrointestinal absorption (HIA) and brain access (BBB) [36]. Despite its simplicity, relying on only two physico-chemical descriptors (WLOGP and TPSA for lipophilicity and apparent polarity), great attention was given to the statistical significance and robustness when constructing this classification model. Illus-

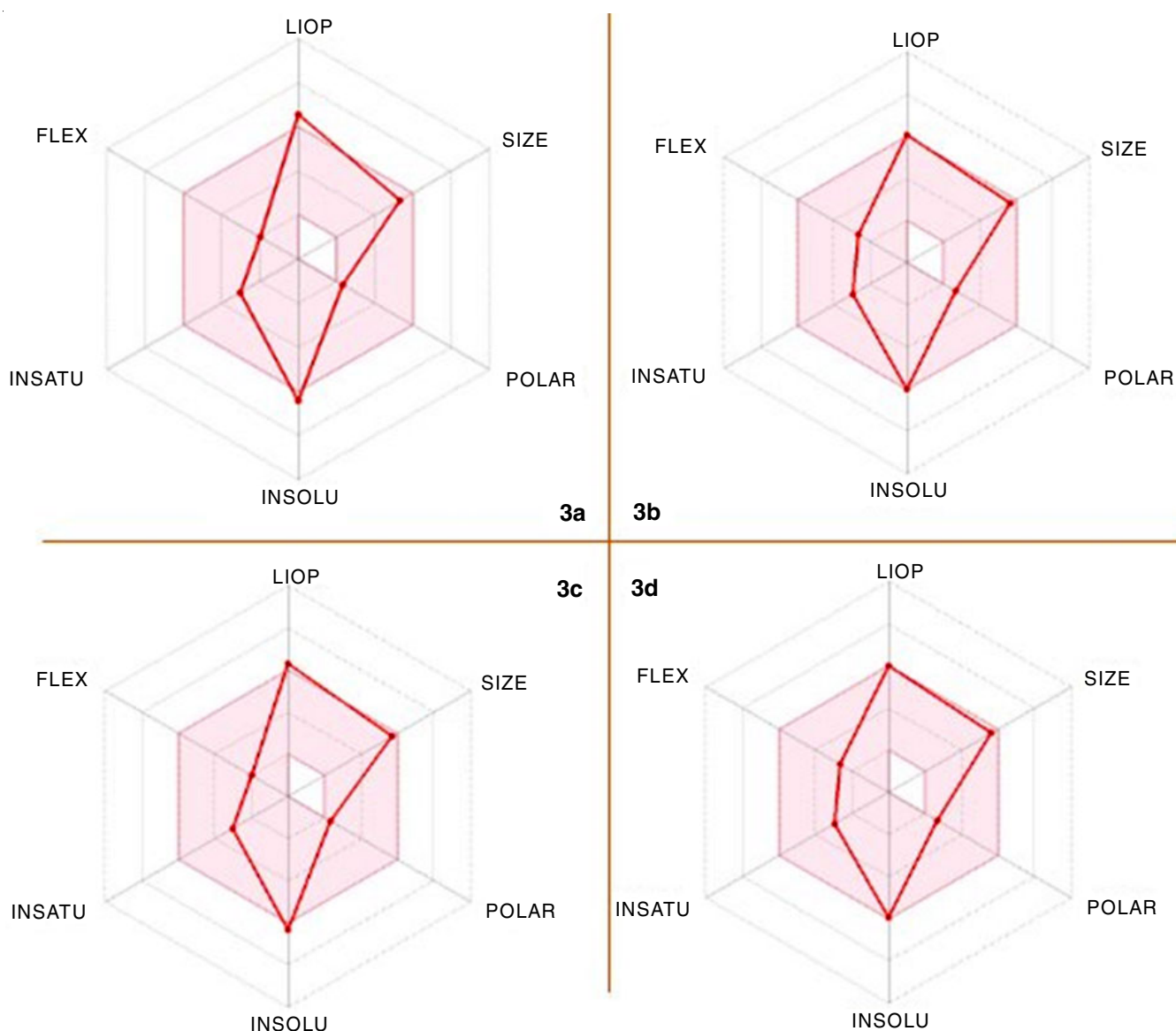


Fig. 1. Bioavailability radar plot of the derivatives: **3a**, **3b**, **3c** and **3d**. POLAR (polarity), LIPO (lipophilicity), INSOLU (solubility), FLEX (flexibility) and INSATU (saturation)

TABLE-2
LIPINSKI AND VEBER FILTERS FOR DRUG-LIKE PROPERTIES [DRUG-LIKENESS]

Compound	m.w.	Clog P*	Log D [#]	^a HBA	HBD	RBs	tPSA	Ro5 (Y/N)
3a	441.19	3.036	1.755	2	0	3	27.96	Y
3b	501.21	2.579	1.305	3	2	4	46.42	Y
3c	475.15	3.755	2.305	2	0	5	29.02	Y
3d	471.43	3.080	1.655	3	1	4	37.19	Y
[†] Metronidazole	171.15	-0.175	0.40	5	2	3	87.64	Y
[‡] Ornidazole	219.62	-1.19	0.25	5	2	4	87.64	Y

*At pH 7.4; [#]Calculated using ChemAxonLogD predictor; [†]Taken from referred sources; HBA–hydrogen bond acceptor, HBD–hydrogen bond donor, obtained by Marvin Sketch 22.11; RB: Rotatable bonds; Ro5 (Y/N): Rule of five followed or not; Y: Yes; N: No; Veber filter: Rotatable bonds ≤ 10 , tPSA ≤ 140 .

trated in Fig. 2, the egg-shaped classification plot encompasses the yolk, representing the physico-chemical space associated with highly probable BBB permeation and the white area, indicating the physico-chemical space for highly probable HIA absorption. These compartments are not mutually exclusive, while the gray region outside signifies molecules with properties suggesting predicted low absorption and limited brain penetration. The BOILED-Egg approach has demonstrated its ease of interpretation and effective application in molecular design within diverse drug discovery settings. It is important to note that while the BOILED-Egg exhibits broad predictive power across chemical space, its scope is limited to passive penetration through the gastrointestinal wall and BBB. The analyzed representative molecule, particularly **3d** as depicted in Fig. 2, is predicted to be well-absorbed, but without potential brain access (in the white area) and PGP (red dot).

Molecular docking studies: To investigate the interactions between newly synthesized organometallic compounds and the NADP binding site of *Entamoeba histolytica* thioredoxin reductase (EhTrR) (PDB ID: 4CCQ), molecular docking studies were conducted. The 2D structures of all organometallics were converted into energy-minimized 3D structures and utilized for docking simulations. Thioredoxin reductase (TrR) plays a vital role in preventing, regulating and repairing oxidative stress-induced damage in *E. histolytica*. The molecular docking calculations for all organometallics were performed using MOE 2015.10 [44]. The conformation with the lowest binding free energy was selected for further analysis. The docking studies revealed that all organometallics exhibited favourable binding energy towards the target protein, indicating a strong affinity. Various molecular interactions were identified as responsible

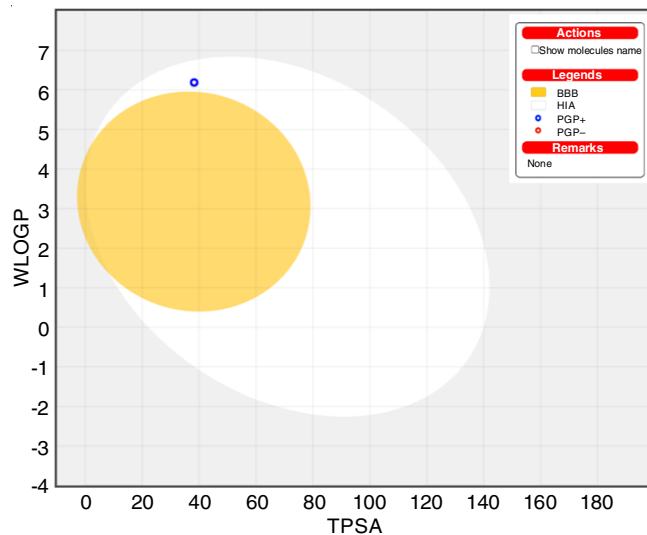


Fig. 2. BOILED egg predictive model for one of the most active compounds **3d**. All the active components displayed similar properties

for this observed affinity. Notably, the molecules demonstrated excellent binding within the active site pocket and engaged in different types of interactions with amino acid residues, as illustrated in the two-dimensional images of compound **3d** (Fig. 3). The docking results prominently identified **3d** as the most active compound based on its energy score and interactions with the target protein. All organometallics displayed docking scores greater than 8.963, surpassing the energy score of reference drugs. Additionally, the lead molecules and their derivatives exhibited favourable ADMET properties and successfully cleared Lipinski's filters for drug-like properties

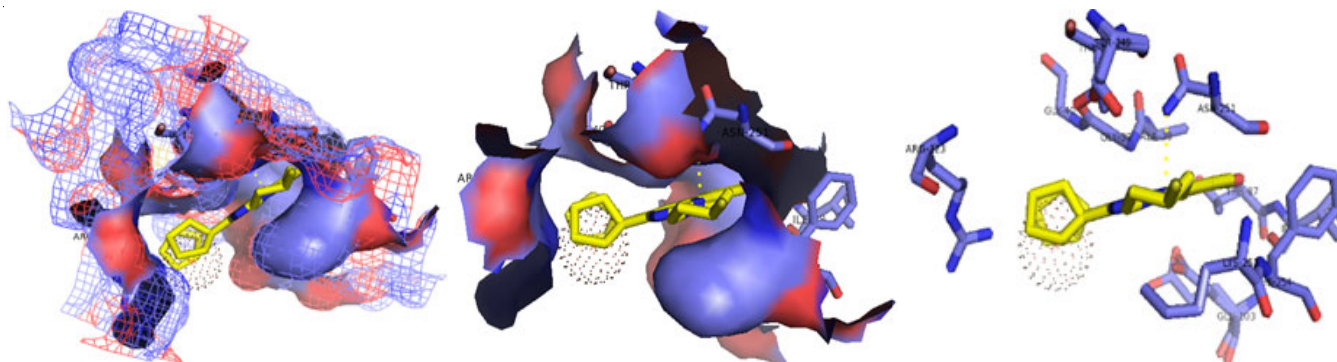


Fig. 3. Docked images of the most active organometallics. Ligand interactions within the active site pocket of the protein 4CCQ, shown as 3D interactions

(drug-likeness). Collectively, these findings offer promising prospects for the development of new ferrocene-based pyrimidine containing organometallics as effective treatment options against *Entamoeba histolytica*.

Thioredoxins are small proteins found ubiquitously and are involved in essential metabolic functions that help maintain the intracellular redox balance. Thioredoxin reductase enzymes are composed of homodimeric proteins, with each monomer containing a NADPH binding domain, FAD domain and an active site that houses a redox-active disulfide [45]. The primary role of thioredoxin reductase is to facilitate the transfer of reducing equivalents between NADPH and thioredoxin in a reversible manner [46]. In the case of *E. histolytica*, thioredoxin reductase (EhTrR) plays a crucial part in metabolic functions by catalyzing the NADP-dependent reduction of amoebic thioredoxins, thereby maintaining intracellular redox balance. Due to its significance, EhTrR has emerged as an attractive target for developing anti-amoebic compounds. Molecules capable of binding to this target are anticipated to exhibit potential anti-amoebic activity.

The molecular docking studies conducted shed light on the excellent binding of the molecules, particularly compound **3d**, within the active site pocket. Notably, compound **3d** demonstrated drug-likeness properties, successfully passing Lipinski's and Veber's filters for drug-likeness and exhibited promising physico-chemical characteristics. Based on these findings, it can be inferred that the novel organometallic compound **3d** holds great potential as a lead molecule for designing more potent anti-amoebic compounds.

Conclusion

Some novel ferrocene-embedded organometallics with pyrimidine moiety were synthesized and evaluated as potential candidates for protozoal chemotherapy. The synthesized organometallics demonstrated excellent ADMET (Absorption, distribution, metabolism, excretion and toxicity) profile, successfully passing Lipinski's filters and exhibiting favourable drug-like properties (drug-likeness). The pharmacokinetic studies indicated efficient clearance from the body, suggesting non-toxic and non-hepatotoxic profiles. The compounds also showed promising oral toxicity values and maximum tolerated doses. Molecular docking studies revealed high docking scores, with compound **3d** displaying the most significant activity. These findings highlight the potential of these organometallic compounds as promising drug candidates for the development of potent antiprotozoal agents.

ACKNOWLEDGEMENTS

This research work was supported by the Deanship of Scientific Research (DSR) at the University of Tabuk, Kingdom of Saudi Arabia through research Grant No. S-0117-1438, for which the authors extended their appreciation.

CONFLICT OF INTEREST

The authors declare that there is no conflict of interests regarding the publication of this article.

REFERENCES

- J. Nasrallah, M. Akhondi, D. Haouchine, A. Marteau, S. Mantelet, P. Wind, R. Benamouzig, O. Bouchaud, R. Dhote and A. Izri, *J. Infect. Public Health*, **15**, 1134 (2022); <https://doi.org/10.1016/j.jiph.2022.08.013>
- D.I. Edwards, *J. Antimicrob. Chemother.*, **31**, 201 (1993); <https://doi.org/10.1093/jac/31.2.201>
- M.M. López Nigro, A.B. Gadano and M.A. Carballo, *Toxicol. In Vitro*, **15**, 209 (2001); [https://doi.org/10.1016/S0887-2333\(01\)00010-8](https://doi.org/10.1016/S0887-2333(01)00010-8)
- N.J. Moreno and R. Docampo, *Environ. Health Perspect.*, **64**, 199 (1985); <https://doi.org/10.1289/ehp.8564199>
- C. Ordaz-Pichardo, M. Shibayama, S. Villa-Trevino, M. Arriaga-Alba, E. Angeles and M. de la Garza, *Antimicrob. Agents Chemother.*, **49**, 1160 (2005); <https://doi.org/10.1128/AAC.49.3.1160-1168.2005>
- A. Bendesky, D. Menendez and P. Ostrosky-Wegman, *Mutat. Res. Rev. Mutat. Res.*, **511**, 133 (2002); [https://doi.org/10.1016/S1383-5742\(02\)00007-8](https://doi.org/10.1016/S1383-5742(02)00007-8)
- A.F. El-Nahas and I.M. el-Ashmawy, *Basic Clin. Pharmacol. Toxicol.*, **94**, 226 (2004); <https://doi.org/10.1111/j.1742-7843.2004.pto940505.x>
- V. Purohit and K.A. Basu, *Chem. Res. Toxicol.*, **13**, 673 (2000); <https://doi.org/10.1021/tx000002x>
- J. Evans, D. Levesque, K. Knowles, R. Longshore and S. Plummer, *J. Vet. Intern. Med.*, **17**, 304 (2003); <https://doi.org/10.1111/j.1939-1676.2003.tb02452.x>
- A. Azam and S.M. Agarwal, *Curr. Bioact. Compd.*, **3**, 121 (2007); <https://doi.org/10.2174/157340707780809590>
- S. Becker, E.R. Houpt and P. Hoffman, *Am. J. Trop. Med. Hyg.*, **84**, 581 (2011); <https://doi.org/10.4269/ajtmh.2011.10-0580>
- G. Jaouen, A. Vessieres and S. Top, *Chem. Soc. Rev.*, **44**, 8802 (2015); <https://doi.org/10.1039/C5CS00486A>
- S. Top, A. Vessieres, C. Cabestaing, I. Laios, G. Leclercq, C. Provot and G. Jaouen, *J. Organomet. Chem.*, **637-639**, 500 (2001); [https://doi.org/10.1016/S0022-328X\(01\)00953-6](https://doi.org/10.1016/S0022-328X(01)00953-6)
- E.A. Hillard, A. Vessières, L. Thouin, G. Jaouen and C. Amatore, *Angew. Chem. Int. Ed.*, **45**, 285 (2006); <https://doi.org/10.1002/anie.200502925>
- D. Hamels, P.M. Dansette, E.A. Hillard, S. Top, A. Vessières, P. Herson, G. Jaouen and D. Mansuy, *Angew. Chem. Int. Ed.*, **48**, 9124 (2009); <https://doi.org/10.1002/anie.200903768>
- X. Wang and Z. Guo, *Chem. Soc. Rev.*, **42**, 202 (2013); <https://doi.org/10.1039/C2CS35259A>
- P. Pigeon, S. Top, A. Vessières, M. Huché, E.A. Hillard, E. Salomon and G. Jaouen, *J. Med. Chem.*, **48**, 2814 (2005); <https://doi.org/10.1021/jm049268h>
- W.A. Wani, E. Jameel, U. Baig, S. Mumtazuddin and L.T. Hun, *Eur. J. Med. Chem.*, **101**, 534 (2015); <https://doi.org/10.1016/j.ejmech.2015.07.009>
- S. Top, C. Thibaudeau, A. Vessières, E. Brulé, F. Le Bideau, J.M. Joerger, M.A. Plamont, S. Samreth, A. Edgar, J. Marrot, P. Herson and G. Jaouen, *Organometallics*, **28**, 1414 (2009); <https://doi.org/10.1021/om800698y>
- D. Plazuk, A. Vessieres, E.A. Hillard, O. Buriez, E. Labbé, P. Pigeon, M.-A. Plamont, C. Amatore, J. Zakrzewski and G. Jaouen, *J. Med. Chem.*, **52**, 4964 (2009); <https://doi.org/10.1021/jm900297x>
- J.A. Carmona-Negrón, A. Santana, A.L. Rheingold and E. Meléndez, *Dalton Trans.*, **48**, 5952 (2019); <https://doi.org/10.1039/C8DT01856A>
- M. Murwih Alidmat, M. Khairuddean, N. Mohammad Norman, A.N. Mohamed Asri, M.H. Mohd Suhaimi and G. Sharma, *Arab. J. Chem.*, **14**, 103304 (2021); <https://doi.org/10.1016/j.arabjc.2021.103304>
- Y. Guo, S.Q. Wang, Z.Q. Ding, J. Zhou and B.F.J. Ruan, *J. Organomet. Chem.*, **851**, 150 (2017); <https://doi.org/10.1016/j.jorganchem.2017.09.032>

24. J. Jadhav, A. Juvekar, R. Kurane, S. Khanapure, R. Salunkhe and G. Rashinkar, *Eur. J. Med. Chem.*, **65**, 232 (2013); <https://doi.org/10.1016/j.ejmech.2013.04.021>
25. W. Guo, J. Zhao, M. Li, T. Hu, Z. Dan, Q. Zhang, L. Ma, S. Zhang and B. Zhao, *Bioorg. Med. Chem. Lett.*, **76**, 129020 (2022); <https://doi.org/10.1016/j.bmcl.2022.129020>
26. V. Finger, M. Kufa, O. Soukup, D. Castagnolo, J. Roh and J. Korabecny, *Eur. J. Med. Chem.*, **246**, 114946 (2023); <https://doi.org/10.1016/j.ejmech.2022.114946>
27. W. Zhan, P. Mao, C. Yuan, Y. Zhang, T. Zhang, Y. Liu, J. Tian and W. Xue, *J. Saudi Chem. Soc.*, **27**, 101590 (2023); <https://doi.org/10.1016/j.jscs.2022.101590>
28. M. Al-Anazi, M. Khairuddean, B. O. Al-Najjar, M. Murwih Alidmat, N. Nur Syazni Nik Mohamed Kamal and M. Muhamad, *Arab. J. Chem.*, **15**, 103864 (2022); <https://doi.org/10.1016/j.arabjc.2022.103864>
29. H. Parveen, R.A.S. Alatawi, M.A. Alsharif, M.I. Alahmdi, S. Mukhtar, S.A. Khan, S. Hasan and A.U. Khan, *Appl. Organomet. Chem.*, **32**, e4257 (2018); <https://doi.org/10.1002/aoc.4257>
30. H. Parveen, M.A. Alsharif, M.I. Al-Ahmdi, S. Mukhtar and A. Azam, *Appl. Organomet. Chem.*, **32**, e4261 (2018); <https://doi.org/10.1002/aoc.4261>
31. H. Parveen, R.A.S. Alatawi, N.H. El Sayed, S. Hasan, S. Mukhtar and A.U. Khan, *Arab. J. Chem.*, **10**, 1098 (2017); <https://doi.org/10.1016/j.arabjc.2015.05.002>
32. H. Parveen, S. Mukhtar and A. Azam, *J. Heterocycl. Chem.*, **53**, 473 (2016); <https://doi.org/10.1002/jhet.2427>
33. H. Parveen, F. Hayat, S. Mukhtar, A. Salahuddin, A. Khan, F. Islam and A. Azam, *Eur. J. Med. Chem.*, **46**, 4669 (2011); <https://doi.org/10.1016/j.ejmech.2011.05.055>
34. H. Parveen, F. Hayat, A. Salahuddin and A. Azam, *Eur. J. Med. Chem.*, **45**, 3497 (2010); <https://doi.org/10.1016/j.ejmech.2010.04.023>
35. M.A. Alsharif, N. Ahmed, M. Issa Alahmdi, S. Mukhtar, H. Parveen, R.J. Obaid and A.S.A. Almalki, *J. Saudi Chem. Soc.*, **26**, 101568 (2022); <https://doi.org/10.1016/j.jscs.2022.101568>
36. A. Daina and V. Zoete, *ChemMedChem*, **11**, 1117 (2016); <https://doi.org/10.1002/cmdc.201600182>
37. J.M. Andrews, N. Anand, A.R. Todd and A. Topham, *J. Chem. Soc.*, 2490 (1949); <https://doi.org/10.1039/jr9490002490>
38. D.E.V. Pires, T.L. Blundell and D.B. Ascher, *J. Med. Chem.*, **58**, 4066 (2015); <https://doi.org/10.1021/acs.jmedchem.5b00104>
39. N.A. Meanwell, *Chem. Res. Toxicol.*, **24**, 1420 (2011); <https://doi.org/10.1021/tx200211v>
40. E.H. Kearns and L. Di, *Drug-Like Properties: Concepts, Structure, Design and Methods*, Elsevier, USA (2008).
41. M.P. Gleeson, *J. Med. Chem.*, **51**, 817 (2008); <https://doi.org/10.1021/jm701122q>
42. A. Daina, O. Michielin and V. Zoete, *Sci. Rep.*, **7**, 42717 (2017); <https://doi.org/10.1038/srep42717>
43. H.T. Abdel-Mohsen, A. Abood, K.J. Flanagan, A. Meindl, M.O. Senge and H.I. El Diwani, *Arch. Pharm.*, **353**, 1900271 (2020); <https://doi.org/10.1002/ardp.201900271>
44. Molecular Operating Environment (MOE), 2020.09 Chemical Computing Group ULC, 1010 Sherbooke St. West, Suite #910, Montreal, QC, Canada, H3A 2R7 (2022).
45. D. Mustacich and G. Powis, *Biochem. J.*, **346**, 1 (2000); <https://doi.org/10.1042/bj3460001>
46. D.G. Arias, E.L. Regner, A.A. Iglesias and S.A. Guerrero, *Biochim. Biophys. Acta*, **1820**, 1859 (2012); <https://doi.org/10.1016/j.bbagen.2012.08.020>